IEEE Journal of Microwaves

Received 14 August 2021; revised 13 October 2021; accepted 28 October 2021. Date of publication 30 November 2021; date of current version 7 January 2022.

Digital Object Identifier 10.1109/JMW.2021.3126199

Modulated Metasurfaces for Microwave Field Manipulation: Models, Applications, and Design Procedures

ENRICA MARTINI (Senior Member, IEEE), AND STEFANO MACI (Fellow, IEEE)

(Invited Paper)

Department of Information Engineering and Mathematics, University of Siena, 53100 Siena, Italy

CORRESPONDING AUTHOR: Enrica Martini (e-mail: martini@dii.unisi.it).

This work was supported in part by the Italian Space Agency and the European Space Agency.

ABSTRACT Metasurfaces (MTSs) have emerged in the last years as a promising platform for next generation planar devices in a broad range of frequencies, thanks to their unique field manipulation capability. In particular, in the microwave range this solution is characterized by low-cost, lightweight, and simple integration with electronic circuits, since MTSs can be realized in PCB technology by printing electrically small patches over a dielectric slab. The MTS behavior can then be conveniently described in terms of homogenized boundary conditions of impedance type. Spatial modulation of these boundary conditions allows one to implement a broad class of functionalities, involving space wave or surface wave control, as well as conversion from surface waves to leaky waves. This paper reviews numerical and analytical models, design procedures and microwave applications of modulated MTSs, with particular emphasis on surface wave manipulation, and it discusses expected future developments of this technology.

INDEX TERMS Impedance boundary conditions, leaky wave antennas, metasurfaces, periodic structures, planar antennas, planar lenses, surface waves.

I. INTRODUCTION

Metasurfaces (MTSs) are artificial two-dimensional structures with deeply subwavelength thickness and electrically small unit cells, that can be engineered to control the interaction with electromagnetic fields [1]. They have emerged in the last years as the most promising class of metamaterials (MTMs) in a large variety of engineering applications from microwaves to optics, thanks to the increased fabrication simplicity, lower losses, reduced cost and limited frequency dispersion with respect to their three-dimensional counterpart, the latter typically consisting of resonant unit cells [2].

As for volumetric MTMs, the electromagnetic properties of MTSs can be effectively described in terms of homogenized parameters, thanks to the subwavelength size of the unit cell. Due to the small thickness, however, as a difference from volumetric MTMs, the most appropriate representation is not in terms of bulk constitutive parameters but rather in terms of boundary conditions (BCs) relating the transverse components of the fields. These latter conditions can be expressed in terms of surface polarizabilities, surface susceptibilities or surface impedances/admittances [3], [4]. For a generic MTS, generalized sheet transition conditions [5] provide the most general description. However, in the microwave range, MTSs are generally realized in printed circuit board (PCB) technology, by printing electrically small metallic elements over a dielectric slab [6], while all-metal solutions are preferred at higher frequencies [7].

For MTSs realized in PCB technology, the electromagnetic properties are controlled by properly patterning the metallic layers(s), and the most convenient representation is the one modeling the metallic layer(s) through a penetrable equivalent impedance [8]. By properly designing this equivalent impedance, it is possible to control wave propagation both along the surface and in the surrounding free space. Several applications have been demonstrated in the last years. The earliest applications involved *uniform* MTSs, i.e., MTSs consisting of identical unit cells and therefore conceptually similar to frequency selective surfaces (FSS). Uniform MTSs can

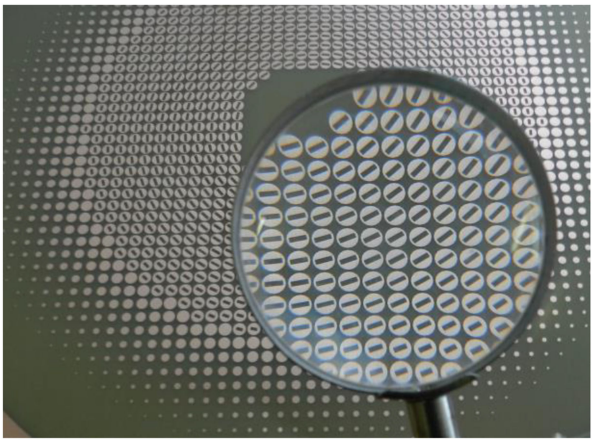

FIGURE 1. Example of modulated MTS with the zoomed view of a region.

be used to control the polarization of radiated fields [9], [10], to realize wide angle impedance matching layers [11]–[13], to enhance absorption [14], to increase antenna directivity or suppress undesired antenna coupling [15], [16]. In these contexts, the novelty of MTSs with respect to FSS and periodic surfaces with unit cell-size comparable with the wavelength are the increased compactness, the improved angular stability, and the reduced coupling through higher order modes in multilayer structures.

In the last decade, it has been shown that new functionalities can be achieved by using *modulated* MTSs, i.e., MTSs presenting a smooth spatial variation of the equivalent impedance. In this case, the model based on homogenized BCs, justified by the small electrical dimension of the unit cell, permits to use simplified and more accurate design approaches. In practice, the modulation is usually achieved by gradually changing the unit cell patterning, while keeping the lattice unchanged (see Fig. 1). By means of a proper spatial variation of the BCs it is possible to control an interacting electromagnetic field, with a number of practical applications that can be grouped into three main categories: *i*) manipulation of radiated waves, *ii)* manipulation of guided waves and *iii)* conversion between guided waves and radiated waves. The first category includes metascreens for beam shaping and routing in both transmission and reflection [17]–[20], space wave cloaks [21], [22] and imaging devices [23], [24]. The second category includes planar waveguides [25], [26], surface wave cloaks [27], beam shifters and splitters [28], planar lenses [29]–[33]. Finally, the third category is represented by modulated MTS antennas [6], [34]–[36].

More recent studies concentrate on active MTSs, with the objective of either obtaining reconfigurability or overcoming some fundamental limitations of passive structures [37]–[39].

This paper offers a review of MTS modeling, design and applications in the microwave range, with particular emphasis on the work performed by the authors' group in the field of surface wave (SWs) manipulation and SW to leaky wave (LW) conversion. Recent comprehensive reviews on MTSs for space-wave manipulations can be found in the literature

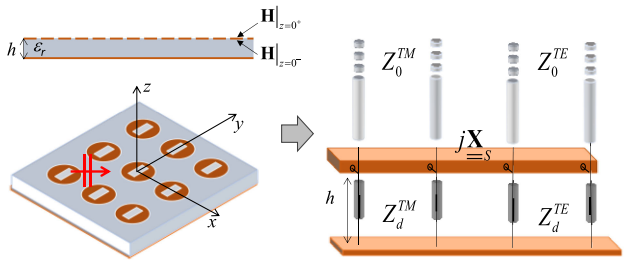

FIGURE 2. Geometry for the periodic MTS and corresponding equivalent transmission line model.

(see for instance [10], [20], [40]–[42]). The paper is organized as follows. Section II introduces the homogenized models used for an effective description of the modulated MTSs. Section III and Section IV deal with SW manipulation and SW to LW conversion, respectively. Reconfigurable MTSs are discussed in Section V. Finally, conclusions are drawn in Section VI.

II. MTS MODELING

In the microwave range, MTSs are typically realized through metallic patterns printed over a single-layer or multilayer dielectric slab. The configuration of major interest for manipulation of guided waves or guided wave-to-leaky wave conversion consists of patches printed over a single, grounded dielectric layer. For this reason, for the sake of simplicity, and without loss of generality, a single dielectric layer will be considered in the following. If needed, the presence of multiple layers can be easily taken into account without changing the general features of the models. Also, we neglect losses, or we consider them through a perturbative approach, which is normally a very good approximation in the microwave frequency range.

A. EQUIVALENT IMPEDANCE

As anticipated in Section I, it is convenient to represent the MTS through homogenized BCs of impedance type, relating the tangential components of the electric and magnetic fields. For a modulated MTS, the definition of the effective BCs at each unit cell relies on a local periodicity assumption, *i.e.*, it is derived from the periodic structure obtained by replicating indefinitely that unit cell. For that periodic structure, the field can be expanded in Floquet Wave (FW) series [43] and the homogenized BC is the one relevant to the dominant FW, thus, associated with the average fields.

The geometry for the periodic structure is represented in Fig. 2. The vanishingly thin patterned metallic layer lies on the *x*-*y* plane of a Cartesian reference system, and it is positioned on top of a grounded dielectric slab with relative permittivity ε_r and thickness *h*. For this structure, the equivalent transmission line model depicted on the right of the same figure can be rigorously defined for the dominant FW. In this model, the ground plane is represented by a short circuit which terminates two branches of equivalent transmission lines, representing

the dielectric slab and associated with the transverse electric (TE, or '*h*') and the transverse magnetic (TM, or '*e*') (with respect to z) modes, while the metallic pattern is represented by a shunt load, which ensures the continuity of the tangential electric field and couples the two transmission lines.

Two different types of impedance BCs can be used to characterize the MTS. The first one is a *penetrable* impedance BC (PIBC), which relates the tangential electric field to the discontinuity of the tangential magnetic field across the metallization as follows

$$\mathbf{E}_t\left(z=0\right)=j\underline{\underline{X}}_S\hat{\mathbf{z}}\times\left[\mathbf{H}_t\left(z=0^+\right)-\mathbf{H}_t\left(z=0^-\right)\right] \quad (1)$$

The penetrable tensor impedance $j\underline{\underline{X}}_S$ only represents the contribution of the patterned metallic layer, and it is therefore weakly dependent on the transverse wavenumber of the interacting field, k_ρ. In the low frequency regime, this reactance will be capacitive or inductive for patch-type or slot-type metallic claddings, respectively. In most of the applications shown in the following, we are interested in the first type of MTSs, since a capacitive reactance allows one to increase the equivalent impedance of a thin grounded slab.

The second type of BC is an *impenetrable* impedance BC (IIBC), which relates the average tangential electric and magnetic fields at $z{=}0^+$ through the tensor impedance $j\underline{\underline{X}}$, which accounts for the contribution of both the patterned metallic layer and the grounded slab

$$\mathbf{E}_t\left(z=0^+\right)=j\underline{\underline{X}}\hat{\mathbf{z}}\times\mathbf{H}_t\left(z=0^+\right) \quad (2)$$

The relationship between $j\underline{\underline{X}}$ and $j\underline{\underline{X}}_S$ expressed in the TM/TE reference system of the interacting wave can be derived from the equivalent transmission line model as

$$\begin{bmatrix}X^{ee} & X^{eh}\\ X^{he} & X^{hh}\end{bmatrix}^{-1}=\begin{bmatrix}X_S^{ee} & X_S^{eh}\\ X_S^{he} & X_S^{hh}\end{bmatrix}^{-1}+\begin{bmatrix}X_{sc}^{e} & 0\\ 0 & X_{sc}^{h}\end{bmatrix}^{-1} \quad (3)$$

where $X_{sc}^{e/h}$ is the TM/TE reactance of the grounded slab, given by

$$X_{sc}^{e/h}=Z_d^{e/h}\tan\left[h\sqrt{k_1^2-k_\rho^2}\right] \quad (4)$$

with

$$k_1=k_0\sqrt{\varepsilon_r}$$
$$Z_d^e=\frac{\zeta_0}{\varepsilon_r}\frac{\sqrt{k_1^2-k_\rho^2}}{k_0}\quad Z_d^h=\zeta_0\frac{k_0}{\sqrt{k_1^2-k_\rho^2}} \quad (5)$$

k_0, ζ_0 being the wavenumber and impedance of free space, respectively.

As apparent from (3), the tensor impedance $j\underline{\underline{X}}$ presents a significant space dispersion, *i.e.*, it exhibits a non-negligible dependency on the transverse wavenumber, due to the contribution of the grounded slab. For this reason, while the PIBC model and the IIBC model are exactly equivalent for a given wavenumber, the first one is more accurate whenever the same BC has to be used for different wavenumbers [44], [45].

It is also noted that the penetrable impedance model can be generalized to a generic multilayer environment and applied also to MTSs operating in transmission. In presence of multiple printed layers separated by small distances, interlayer interactions through higher order FWs should be also taken into account. This can be done by means of a multiport network based on the concept of "accessible modes" [46]. This model neglects the ports associated with MTS-layer Floquet's modes that are sufficiently attenuated at contiguous layers.

The equivalent tensor reactance in eq. (1) is Hermitian in absence of losses, i.e., $\underline{\underline{X}}_S=\underline{\underline{X}}_S^*$, and real and symmetric when the constituent unit cells possess two orthogonal symmetry axes. In the following, we restrict ourselves to this case, which is the one most often encountered in practice. Under this hypothesis, the symmetry axes of the unit cell approximately coincide with the principal axes of the tensor (a small misalignment is present when the symmetry axes of the unit cell are not aligned with the lattice's axes), and the reactance tensor becomes diagonal when the interacting wave is propagating along one of these axes. This means that there is no coupling between the TE and the TM equivalent transmission lines, and the two polarizations can be studied separately, describing the MTS with scalar equivalent impedances corresponding to the diagonal entries of the tensor.

It is noted that, although in this paper the emphasis will be on the manipulation of SWs for which $k_\rho > k_0$, the equivalent transmission line model introduced in this section can also be used to describe the interaction with homogeneous plane waves [47] for MTSs operating in reflection or in transmission. In that case, the quantities of interest are the scattering parameters, which can be readily derived from the equivalent transmission line model [17], [48].

B. DISPERSION ANALYSIS

Uniform impedance BCs (IBCs) support SWs, i.e., inhomogeneous plane waves which are characterized by a transverse wavenumber bigger than the one of free space, and therefore exhibit an exponential decay away from the surface in the z-direction. The equivalent transmission line model introduced in the previous section can be conveniently used to find the dispersion relation of these modes. At a given frequency, the dispersion relation is obtained by solving the following resonance equation with respect to the transverse wavenumber k_ρ:

$$\det\left(\begin{bmatrix}X^{ee} & X^{eh}\\ X^{he} & X^{hh}\end{bmatrix}+\begin{bmatrix}X_0^{e} & 0\\ 0 & X_0^{h}\end{bmatrix}\right)=0 \quad (6)$$

where X_0^e and X_0^h are the TM and TE free-space reactances, respectively, given by

$$X_0^e=\zeta_0\frac{\sqrt{k_\rho^2-k_0^2}}{k_0}\qquad X_0^h=\zeta_0\frac{k_0}{\sqrt{k_\rho^2-k_0^2}} \quad (7)$$

A similar dispersion analysis can be performed for a parallel plate waveguide with one wall loaded by an MTS; in that

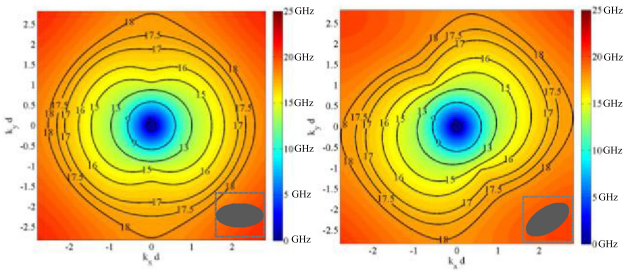

FIGURE 3. Examples of isofrequency dispersion curves for elliptical patches from [50]. The unit cell geometry is shown in the inset in the bottom right corner. All the frequencies are in GHz.

case, the free-space tensor reactance must be replaced by the contribution of the metallic cover, which is analogous to the one defined for the grounded slab.

In general, the SW wavenumber depends on the propagation direction in the transverse plane; the complete description of the MTS dispersion characteristics is therefore given in terms of isofrequency dispersion curves, representing the transverse wavenumber as a function of the propagation direction for different frequencies. However, when the constituent unit cells of the MTS are characterized by a high degree of symmetry (e.g., circular or annular patches), the equivalent penetrable impedance tensor is diagonal with equal on-diagonal entries, and the SW propagation characteristics are nearly independent from the propagation direction (a residual weak dependency may be due to the effect of the rectangular lattice), and the MTS is said *isotropic*. The isofrequency dispersion curves for isotropic MTSs are concentric circles, and do not provide additional information with respect to ordinary dispersion diagrams representing the transverse wavenumber as a function of the frequency. On the other hand, when the constituent unit cell possesses a lower degree of symmetry (e.g., only two orthogonal axes of symmetry), the MTS is said to be *anisotropic*. In this case, the equivalent penetrable impedance is generally represented by a full tensor, and isofrequency dispersion curves have a more complex, frequency dependent shape. Since the real part of the Poynting vector is orthogonal to these curves [49], it is not in general aligned with the phase velocity, except along the principal planes. Two examples of isofrequency dispersion curves, relevant to elliptical patches, are shown in Fig. 3. There, color maps represent, for any spectral point, the frequency of the dominant SW (in GHz). The analysis is performed for a unit cell of side 3 mm, consisting of an elliptical patch printed over a grounded dielectric slab with thickness 1 mm and relative permittivity 9.8. As can be seen, the isofrequency dispersion curves are isotropic for very low frequencies, then they become elongated along the major axis of the ellipse (meaning that the transverse wavenumber is larger for propagation along that direction). At higher frequencies, dispersion is also affected by the square lattice, leading to different shapes of the curves in the two cases.

The current distribution of the SW mode is given by the eigenvector corresponding to the null eigenvalue of the matrix in eq. (6), and it corresponds, in the most general case, to a hybrid mode (not purely TM nor purely TE). However, the TM nature prevails in the low frequency range, due to the dominance of the inductive contribution from the grounded slab. In fact, for electrically thin grounded dielectric slabs, the first mode has no cut-off and it is TM polarized. In the following, when not otherwise specified, we consider only this mode and we suppose to operate in the unimodal band.

In the particular case when the two equivalent transmission lines are decoupled, the supported modes are either purely TM or purely TE also at higher frequencies. This happens for all the propagation directions in isotropic MTSs and in any case for incidence along a principal axis.

For both isotropic and anisotropic MTSs, it is sometimes convenient to define an effective refractive index given by the ratio of the transverse wavenumber and the free-space wavenumber

$$n_{eq} = \frac{k_\rho}{k_0} \tag{8}$$

For anisotropic MTSs, this quantity is direction-dependent, while for isotropic MTSs it is related to the TM equivalent impenetrable reactance as follows

$$n_{eq} = \sqrt{1 + \left(\frac{X^{ee}}{\zeta_0}\right)^2} \tag{9}$$

C. MODULATED METASURFACE IMPLEMENTATION

In patch-based MTSs, IBC modulation is realized by gradually changing the size, shape, and/or orientation of the patches in adjacent unit cells. The size of the unit cells is kept constant throughout the MTS, and it is normally selected in the range [$\lambda/10$, $\lambda/5$], where λ is the free-space wavelength at the central frequency of the operative bandwidth. A homogenized impedance value is assigned to each unit cell based on the aforementioned local periodicity assumption. This latter allows one to restrict the analysis to a single unit cell with periodic BCs, with a significant reduction of the computational burden.

Although approximated, the approach based on the local periodicity assumption has been found to be very accurate for smoothly varying impedance profiles. Notice that the local periodicity assumption is used to retrieve the local equivalent impedance, and not to predict the local behaviour of the MTS. This allows one to correctly account for the spatial variations of the MTS through the modulation of the equivalent impedance. For instance, in [45] it is shown how the field polarization in a single unit call can be affected by the presence of different elements in adjacent unit cells. This effect can not be predicted based on the analysis of the local periodic problem, but it is correctly modelled by associating to each unit cell the homogenized impedance corresponding to the local periodic problem.

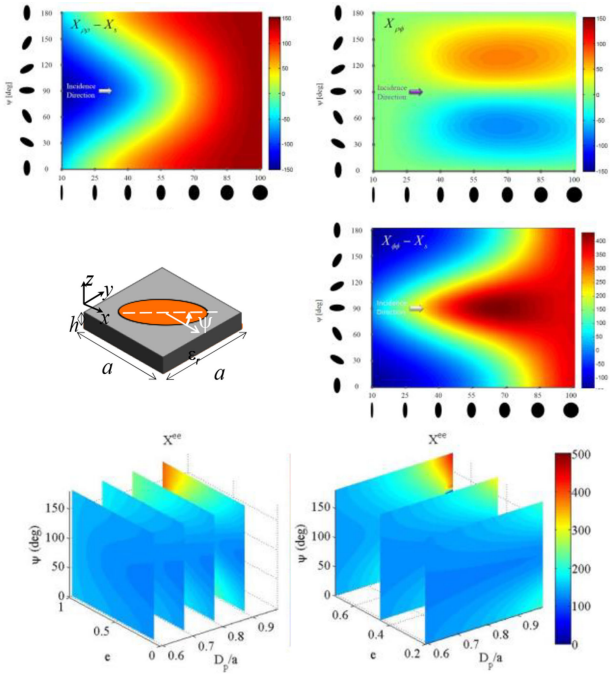

FIGURE 4. Examples of 2D and 3D impedance maps for elliptical patches. D_p represents the major axis of the ellipse and η the ratio between minor and major semiaxes.

Similarly, local periodicity approximation is also used at the synthesis level, that is, for the practical patch implementation of a desired impedance profile. In this case, different unit cells are studied in a periodic environment to construct a database relating the equivalent impedance or the effective refractive index to one or more geometrical parameters of the patches. Then, the element of the database that reconstructs the needed impedance tensor with the minimum error is found through a least square minimization process. It is noted that the database construction represents a sort of pre-processing step that can be re-used in the design of different devices. Furthermore, in practice, only a few samples of the parameter-space are directly calculated, and an interpolation is next used to create a denser database.

A single geometrical parameter is usually sufficient to characterize isotropic unit cells (e.g., the radius of a circular patch), while more parameters are needed for anisotropic MTSs. Typically, these may include two parameters that describe a characteristic size of the patch along the symmetry axes and an angle which describes the rotation of the patch inside the unit cell. This latter parameter mostly influences the orientation of the principal axes of the reactance tensor, while the previous ones mainly affect its principal values. Examples of multidimensional impedance maps are shown in Fig. 4.

Some examples of unit cells are shown in Fig. 5. The choice of the patch shape depends on a number of factors, including the required range of reactance and anisotropy, the impact of ohmic losses, the operative frequency and frequency bandwidth and the fabrication tolerances. A discussion on this point is reported in [36].

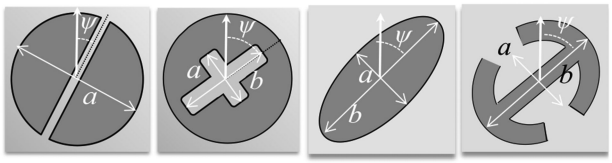

FIGURE 5. Examples of unit cell geometries with two orthogonal symmetry axes, with the indication of the relevant geometrical parameters for impedance maps generation.

Depending on the targeted application, these databases are generated at an assigned transverse wavenumber, solving a driven problem (this is for instance the case when the MTS is used to control reflection or transmission of plane waves) or at the resonance wavenumber, solving an eigenvalue problem (this is the case when the MTS is used to control the propagation of SWs). In the second case, the extraction of the equivalent impedance can be performed with the approach presented in [46], which implements a Method of Moments (MoM) in the spectral domain and extracts the homogenized impedance from the equivalent transmission line relevant to the fundamental FW. When dealing with multilayer structures (e.g., in MTSs operating in transmission) it is possible to use independent maps for each layer, provided that interactions through higher order FWs are negligible (this is usually the case when the interlayer distance is larger than the transverse size of the unit cell). If interactions through higher order FWs are not negligible, multidimensional maps including the geometrical parameters of all the layers should be considered. In this case, it could be convenient to directly create maps for the scattering coefficients instead of for the equivalent impedances.

For certain patch shapes, approximated analytical expressions of the equivalent impedance are available [51], [52]. In other cases, the MoM analysis can be performed with few entire domain basis functions with improved efficiency and precision [50], [53]. In particular, the basis functions proposed in [50] for elliptical patches have a simple closed-form expression in the spectral domain, which makes the application of the spectral MoM extremely fast and accurate.

D. MODULATED METASURFACE ANALYSIS

The analysis of a device based on modulated MTSs is an intrinsically multiscale problem. In fact, the overall device is typically several wavelengths in size, and it consists of a large number of sub-wavelengths elements. When applying a numerical method, these elements, in turn, should be finely discretized in order to correctly describe their near-field interactions. This leads to a very large number of unknowns, with potential problems of ill-conditioning. In order to overcome this problem, it is convenient to perform a full-wave analysis of the "homogenized" structure, *i.e.*, the structure where the metallic cladding is modelled though a continuously spatially varying PIBC. This approach allows one to get rid of the fine details of the single elements, while still accurately describing the electromagnetic behavior of the structure. Furthermore, it

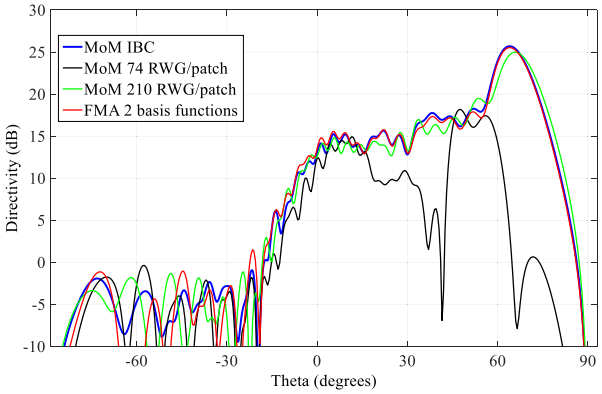

FIGURE 6. Co-polar directivity pattern of an MTS antenna radiating a sectorial secant-type beam: comparison between the Fast Multiple Approach with entire domain basis functions, a MoM with RWG basis functions and a MoM based on continuous BCs (from [58]).

can be shown that a numerical discretization scheme based on an integral formulation yields a stable procedure and accurate results for the PIBC model, as opposed to the IIBC model [44]. The efficiency of the analysis of the homogenized structure can be further increased by using properly defined entire domain basis functions [54]–[57]. In particular, the basis functions proposed in [54] are shaped as Gaussian-type rings with small width and linear azimuthal phase. The analytical form of their spectrum allows for a closed-form evaluation of the MoM impedance matrix's entries, thus, significantly accelerating the simulation. The same basis functions can also be used to analyze (multilayer) MTSs operating in transmission [56].

The full wave simulation at homogenized impedance model provides good accuracy with a limited computational cost (especially if entire domain basis functions are used), and, therefore, it can be effectively used for the design/optimization of MTS-based devices. Anyway, the analysis of the actual patch structure is finally required for assessing the performances, analyzing the frequency behavior, and verifying the sensitivity to construction tolerances. An efficient approach to perform this step is presented in [58]: it uses the two-dimensional version of the Fast Multipole method to accelerate the MoM solution, and entire domain basis functions to describe the current on each patch. For MTSs consisting of elliptical patches, using the basis functions introduced in [50] only two basis functions per patch are sufficient to obtain an accurate result, as illustrated in Fig. 6. That figure reports the far field pattern of an MTS antenna radiating a sectorial beam with secant-type envelope, covering a view angle comprised between 0° and 65°. The results provided by the Fast Multiple approach (FMA) with entire domain basis functions are compared with the ones obtained by applying a MoM with Rao-Wilton-Glisson (RWG) basis functions and different numbers of triangular elements in each elliptical patch, and with the results provided by the MoM code based on continuous BCs [54]. As can be seen, the MoM with RWG basis functions converges to the result with only two entire domain basis functions when the number of RWG basis functions is increased. In turn, this latter result is very close to the one provided by the MoM code based on continuous BCs.

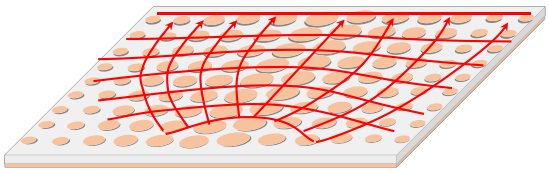

FIGURE 7. SW wavefront shaping through MTS modulation: a progressive reduction of the effective refractive index towards the periphery causes the rays bending towards the central region.

III. GUIDED WAVE MANIPULATION

Modulated MTSs have been successfully used to control the propagation path, phase front shape and polarization of guided waves. In particular, MTSs can be employed to realize planar waveguides for 2-D wireless power transmission, for feeding radiating structures like leaky-wave antennas, and in general for controlling in-plane propagation.

An alternative application is based on the use of MTS lining on the inner walls of closed waveguides to control transverse field distribution and/or polarization. These two applications are addressed in the following. More recently, solutions based on dual MTSs have also been suggested for the realization of topologically protected waveguides, where the propagating mode is inherently protected from backscattering by fabrication defects or sharp bends of the propagation channel [59]–[60].

A. PLANAR WAVEGUIDES AND DEVICES

As illustrated in Section II, a uniform MTS supports the propagation of a bound SW, and it represents therefore an open planar waveguide. Confined propagation can be obtained by bordering a region of high impedance by two regions of lower impedance [25]. A closed MTS-based planar waveguide is obtained by loading one wall of a parallel plate waveguide with an MTS [33].

In both open and closed MTS-based planar waveguides, in the presence of a uniform MTS the wave will propagate along rectilinear paths, with the phase velocity dictated by the effective refractive index. In analogy with space waves in graded index volumetric materials, by spatially modulating the effective refractive index of the MTS it is possible to control the SW wavefront, addressing the local wavevector along not-rectilinear paths. This effect, illustrated in Fig. 7, can be used to design planar devices (e.g., for antenna feeding networks) characterized by low losses, high integrability, extremely low thickness and high design flexibility. A general methodology, denoted as "Flat optics for SWs" has been developed for the description of ray paths, ray velocity, and transport of energy in this kind of devices [61]. The design of planar structures based on modulated MTSs can also be performed in the framework of Transformation Electromagnetics or Transformation Optics [63], [67]–[63], analogously to what

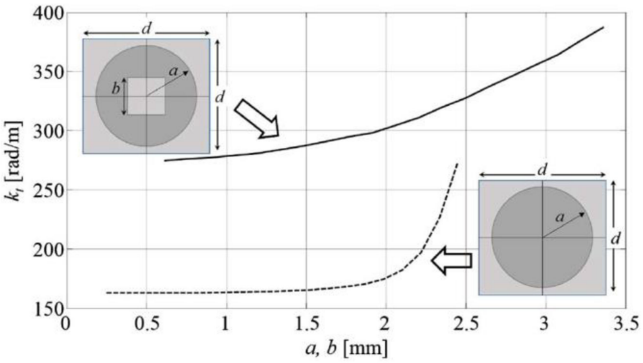

FIGURE 8. Wavenumber maps at 7.5 GHz as a function of patch radius for circular patches (dashed line) and as a function of the square slot side for a slotted circular patch with radius equal to 2.45 mm (continuous line) [63]. The dielectric substrate has a thickness 1.575 mm and relative permittivity 9.8, d = 5 mm.

has been done for volumetric metamaterials [68], [69]. In this case, the ray paths can be conveniently controlled without the use of ray tracing [61].

In the context of guided wave manipulation, isotropic MTSs allow for a simplified description, and they will be considered first. On the other hand, the introduction of anisotropy allows for additional effects, not achievable with isotropic MTSs, as it will be discussed later.

1) ISOTROPIC MTS

The dominant SW mode supported by an *isotropic* MTS can be equivalently characterized either through a scalar impedance or through an effective refractive index, thanks to eq. (9). In a *modulated* MTS these quantities are a function of the transverse coordinates, and the SW propagation is ruled by an eikonal equation, which relates the gradient of the phase term to the equivalent refractive index [61]. Analogously to what happens in volumetric graded index materials, the propagation path of the SW ray-field can therefore be found invoking the Fermat's principle of minimum optical path. The real part of the Poynting vector has zero component orthogonal to the MTS and it is aligned with the transverse wave vector, i.e., it is orthogonal to the phase front.

The design of a planar device based on isotropic MTSs starts from the definition of the desired effective refractive index profile, and it continues with the implementation of this profile through a distribution of patches over a given grounded slab. For a given patch shape, this is done through proper maps linking the effective refractive index to the geometrical parameters of the patch. Since the equivalent refractive index is univocally related to the impenetrable impedance through eq. (9), impenetrable impedance maps can be used in this phase, provided that the impenetrable impedance is calculated at the local resonance.

An example of maps, relevant to circular patches and circular patches with a square hole, is reported in Fig. 8 [63]. Notice that the hole, by extending the path length of the currents, allows one to obtain higher values of the effective refractive index.

The correspondence between space wave propagation in graded index isotropic media and SW propagation over a modulated isotropic MTS can be exploited to derive the refractive index distribution of planar devices from the one of their three-dimensional counterparts. In the last years, various designs and realizations of planar lenses based on this approach have been proposed [29]–[32].

Fig. 9 illustrates examples relevant to a Luneburg Lens, a Maxwell's fish-eye lens [61] and a generalized Maxwell's fish-eye lens [62]. All devices have been designed at 7.5 GHz and they have a radius $a = 125$ mm (3λ) in cases (a) and (b), and $a = 250$ mm (6λ) in case (c). The implementation of the required variation of effective refractive index is done by using the maps shown in Fig. 8.

2) ANISOTROPIC MTS

Anisotropy allows for new interesting phenomena, that further broaden the class of realizable planar devices. In particular, the application of transformation electromagnetics to design MTS devices ([64], [65]) leads to anisotropic BCs whenever the applied geometrical transformation is not conformal. An example is provided by the SW beam shifter presented in [61], obtained by adapting to MTSs the solution proposed in [69] for volumetric metamaterials. By mirroring the patch arrangement of the beam shifter, it is also possible to design beam splitters, as the one shown in Fig. 10 ([61], [64], [70]). There, a SW beam is generated by exciting the structure with 7 horizontal electric dipoles with tapered amplitude. This device exploits the capability of anisotropic MTSs to support SWs propagating with different directions of power flow and phase velocity. Anisotropy may also enable the design of multifunctional devices [71].

B. CLOSED WAVEGUIDES WITH MTS WALLS

MTSs can also be used to tailor the properties of closed guiding structures. For instance, MTSs can be used to miniaturize waveguides and resonators [72]. Furthermore, the use of anisotropic MTS walls in closed waveguides also allows for the control of the field polarization [75]. This effect has been successfully exploited to design MTS-based hybrid mode feed horns [76]–[78], which represent a compact and low-cost alternative to corrugated horns. In this case, the entries of the anisotropic MTS impedance are designed to satisfy the balanced condition that ensures zero cross-polarization. An example of conical horn with MTS walls and relevant radiation pattern is shown in Fig. 11 (from [78]).

IV. LEAKY WAVE GENERATION AND CONTROL

Another important application of modulated MTSs is in the realization of LW antennas. In this case, a locally periodic modulation of the equivalent impedance BCs is designed to convert a SW launched by a feeder into a LW with prescribed characteristics.

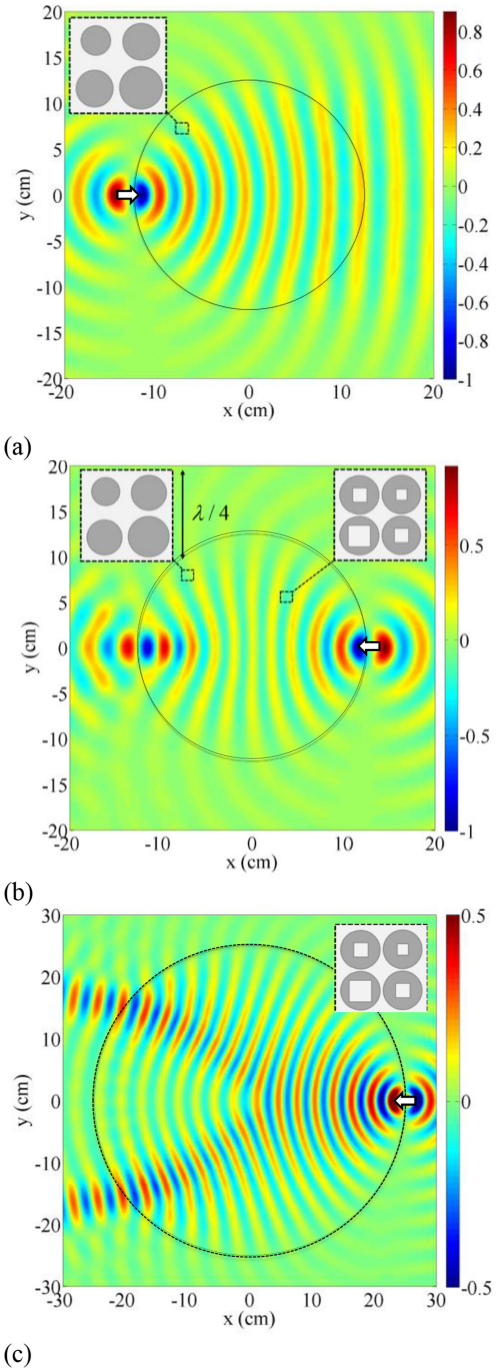

FIGURE 9. Vertical electric field distribution obtained through full wave simulations for planar MTS based: (a) Luneburg Lens, (b) Maxwell fisheye lens, (c) generalized Maxwell fisheye. Zoomed views of the patch layouts are shown in the insets. The circumference delimits the printed region, surrounded by the bare slab. Excitation is provided by a horizontal dipole shown by a white arrow.

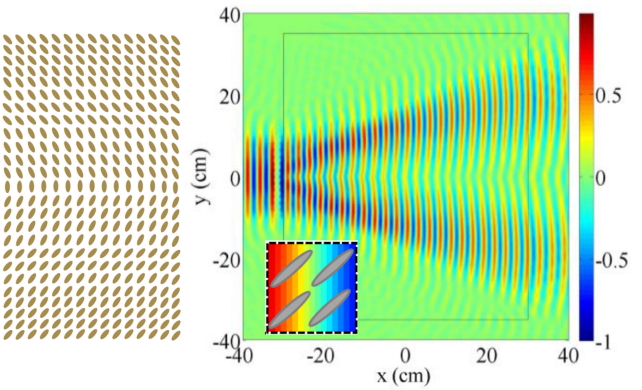

FIGURE 10. Full-wave simulation of a beam splitter (real part of the vertical component of the electric field) whose design is obtained by symmetrizing the structure presented in [61] and realized with an elliptical patch MTS. The left part shows the patch arrangement in the central region, with a zoomed view in the inset.

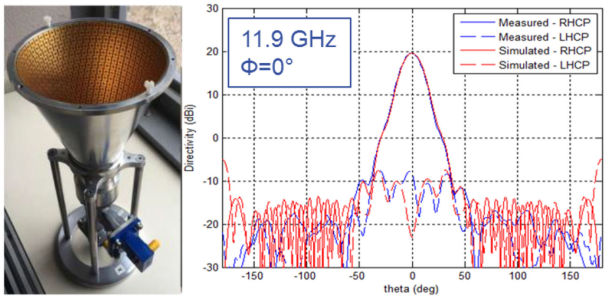

FIGURE 11. Conical horn with MTS walls and relevant simulated and measured radiation pattern from [78].

A. PHENOMENOLOGY

The electromagnetic field supported by an MTS with a periodic modulation can be represented in terms of a FW series. This FW series is associated with the modulation period, and it should not be confused with the one introduced in Section II, whose reference period is the size of the MTS unit cell. Indeed, the phenomenology of a periodically modulated MTS can be conveniently described at homogenized impedance level, without any reference to the unit cells used for MTS implementation. In particular, if the impedance varies sinusoidally along a given direction, it can be assumed as a first approximation that the 0-indexed FW wavenumber coincides with the one of the SW supported by the average impedance, k_ρ. Then, the modulation period d can be chosen so as to have only the -1-indexed mode falling in the visible range, *i.e.*, $|k_\rho - \frac{2\pi}{d}| < k_0$, corresponding to radiation in a direction forming an angle θ with the normal to the surface, with $k_\rho - \frac{2\pi}{d} = k_0 \sin\theta$. The radiation direction depends therefore on the relationship between the modulation period and the SW wavelength: it is broadside when they coincide, forward or backward if the period is bigger or smaller than the SW wavelength, respectively. In practice, the FWs wavenumbers will be slightly perturbed with respect to this simplified picture, with an imaginary part accounting for the power lost due to radiation. This perturbation can be accurately determined by solving the homogenized periodic problem with the approach introduced in [79] for scalar impenetrable BCs and generalized to tensor penetrable impedance model in [80]. Basically, the solution is found by expanding the currents in

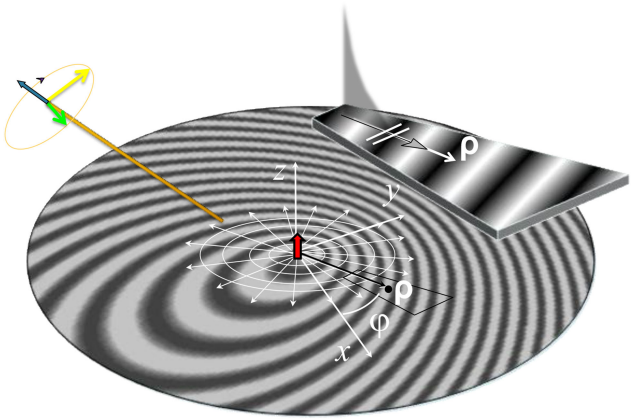

FIGURE 12. **Typical modulated MTS antenna configuration and illustration of the canonical problem.**

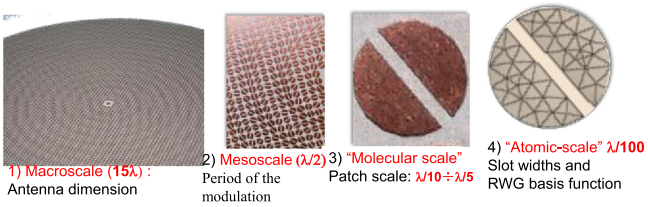

FIGURE 13 **Illustration of the multiple scales involved in modulated MTS antennas.**

FWs with unknown coefficients and imposing the boundary conditions at the MTS. After projecting the resulting equation into the FW basis, a determinantal equation is obtained for the complex propagation wavenumber.

It is noted that, in general, a sinusoidal modulation will excite a number of evanescent modes in addition to the radiating −1-indexed mode. These modes, however, will not contribute to radiation, except possibly for a diffraction contribution originating at the antenna edge. It is also possible to define modulation profiles supporting only the 0-and the −1-indexed modes, as shown in [73], [74].

The mechanism described above is the fundamental brick for the design of radiating structures based on modulated MTSs. The typical configuration of a modulated MTS antenna is illustrated in Fig. 12: a central coplanar feed launches a SW with a cylindrical wavefront over an MTS characterized by (tensor) impedance BCs with a locally periodic modulation. The interaction with the modulated surface transforms the SW into a LW according to the previously defined mechanism. The radiating aperture field can therefore be identified with the −1-indexed term of the local FW expansion. By properly shaping the local modulation of the BCs it is therefore possible to control the amplitude (through modulation depth), phase (through modulation period) and polarization (through anisotropy) of the radiating field, with an extreme flexibility in the antenna design. The resulting radiating structure is characterized by extremely low profile, low weight, reduced losses, and simple inexpensive fabrication.

B. DESIGN PROCEDURE

The design of modulated MTS antennas can not be performed with an optimization procedure based on general purpose simulation tools, due to the intrinsic numerical complexity of the problem. In fact, the description of modulated MTS antennas involves multiple scales, as illustrated in Fig. 13: the overall antenna size, usually consisting of several wavelengths; the modulation period, comparable with the wavelength; the size of the constituent unit cells for MTS implementation, which is a fraction of the wavelength; and finally the size of the elements used in the numerical discretization of the elements inside each unit cell, which is a small fraction of the unit cell size. In order to develop an effective design procedure, it is necessary to properly address each one of these scales.

To this end, our group has developed the procedure illustrated in Fig. 14: the design of the continuous impedance modulation is first done in pseudo-analytical form through the Flat Optics theory presented in [81], which is based on the local canonical problem of a sinusoidally modulated impedance surface [82]. An alternative design approach, not based on the assumption of a locally sinusoidal modulation, is presented in [83]. Then, the resulting continuous impedance layout is analysed with the full-wave code with entire domain basis functions presented in [54], and optimization is performed at this level, if needed. When the performances are satisfactory, the impedance profile is implemented through patches by following the procedure described in previous sections. Finally, full-wave analysis can be performed as a final verification. The strength of this approach relies on the fact that the optimization can be performed at homogenized impedance level, with no need to account for the fine patch details, thus, with a low computational complexity. The results provided by this model are very close to the ones provided by the full-wave analysis of the corresponding patch implementation. An example is shown in Fig. 15, where the results of the two analyses are compared for a broadside beam modulated MTS antenna. As can be seen, the homogenized model provides very accurate results also for the far lobes, which also validates the local periodicity assumption on which the MTS implementation is based.

The final full wave analysis can also be used to evaluate the sensitivity to materials/fabrication tolerances an to verify the frequency behaviour. Being the MTS unit cell sub-resonant, the equivalent impedance normally exhibits a quite slow variation with frequency; however, the operative bandwidth of modulated MTS antennas is limited by the LW frequency-scanning, leading to a decrease of the antenna directivity away from the design frequency. As a general rule, lower average impedances lead to larger bandwidths. An approach to enlarge the bandwidth is presented in [77].

C. EXAMPLES OF DESIGN AND REALIZATION

The design procedure presented in the previous section has been successfully applied to design several antennas with

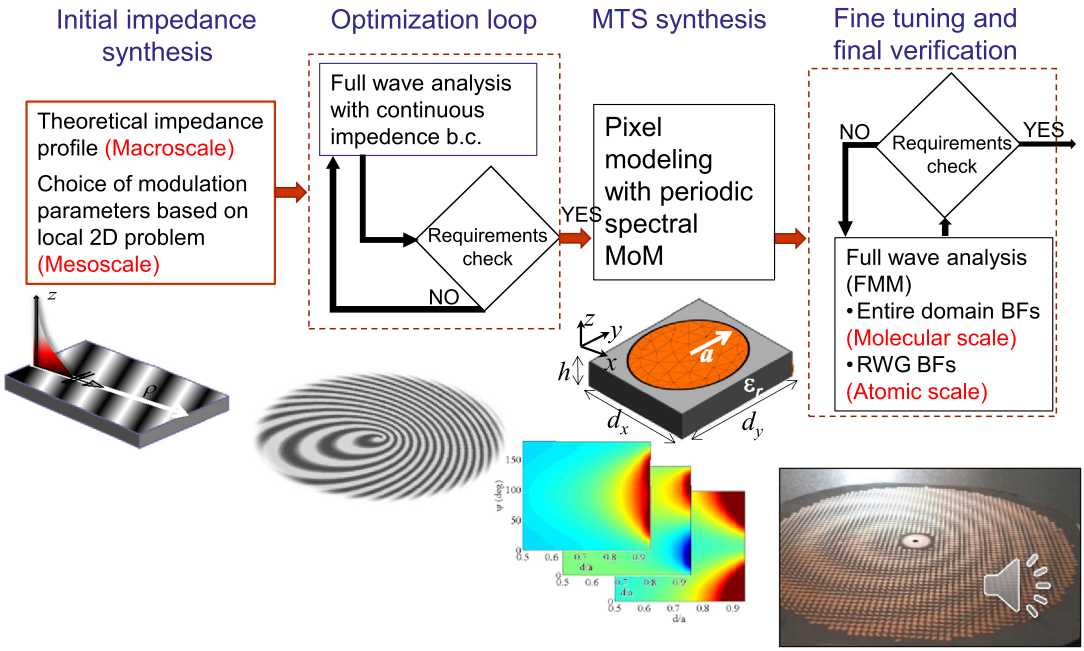

FIGURE 14. Design procedure for modulated MTS antennas.

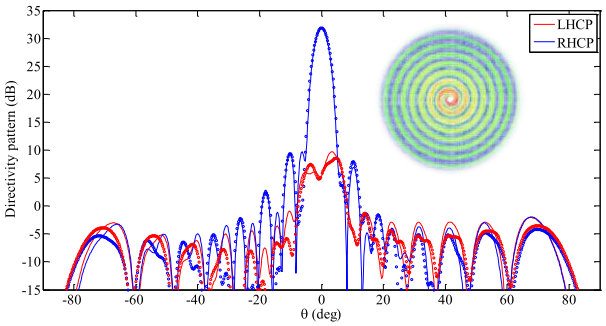

FIGURE 15. Radiation pattern of a broadside beam modulated MTS antenna: comparison between the results of the simulation of the continuous impedance profile through [54] (dotted lines) and of the full-wave analysis of the patch implementation of the same profile. The inset shows the current distribution on the patches.

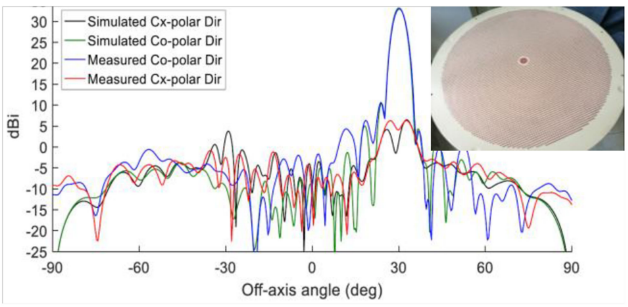

FIGURE 16. Squinted beam modulated MTS antenna operating at 20 GHz: comparison between simulated and measured radiation pattern.

different pattern shapes and performances [35], [36], [82]. Just a couple of examples are reported here. Both of them have been designed by the company Wave Up.

Fig. 16 shows the picture and radiation pattern of an antenna prototype designed for SatCom applications in the Ka band. The antenna has a diameter of 37 cm and it is realized on an Arlon TC600 substrate, with thickness 0.762 mm and relative permittivity 6.15. The measured maximum directivity at 20 GHz is 34 dB. The −1 dB and −3 dB directivity bandwidths are around 2% and 4%, respectively. The antenna is fed at its centre by a vertical monopole connected to a coaxial cable, surrounded by some annular patches designed to obtain impedance matching at the input port while simultaneously maximizing the power launched as SW. Despite the complexity of the MTS layout, involving tens of thousands patches, a very good agreement is obtained between simulations and measurements.

Fig. 17 shows a Ka-band broadside beam MTS antenna designed to have a high aperture efficiency. The antenna is realized on a Rogers RO3003 substrate, characterized by a thickness of 0.762 mm, relative permittivity 3 and loss tangent 0.001. The radius of the antenna is 13.5 wavelengths at the central frequency, and measured directivity is more than 37 dB, corresponding to an aperture efficiency of 80%. Losses are less than 1 dB. The −1 dB and −3 dB directivity bandwidths are around 2.8% and 4.6%, respectively. It is noted that in this case the product bandwidths-directivity is significantly larger than in the previous case, thanks to the use of a lower average impedance.

As can be seen from the prototypes' pictures, the two antennas have very similar general structures, the beam shaping being only provided by the patches' layout.

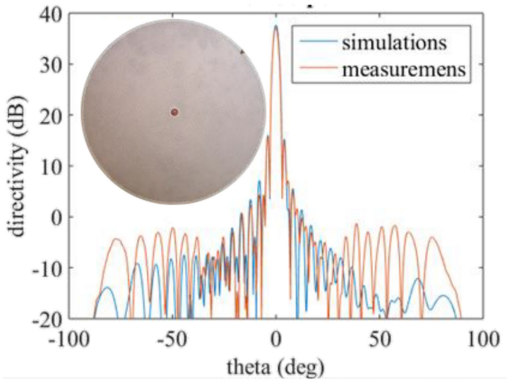

FIGURE 17. High efficiency broadside beam modulated MTS antenna operating at 29.75 GHz: comparison between simulations and measurements [36].

V. RECONFIGURABLE METASURFACES

In recent years, time-varying MTSs, providing the degree of freedom to dynamically change their behavior, have attracted great attention and have become one of the most promising research fields [37]–[39]. For antennas, this provides the possibility of performing electronic beam scanning without the need of lossy and expensive phase shifters. Hence, dynamic metasurfaces are promising new platforms for 5G communications, remote sensing and radar applications. Furthermore, by the insertion of active elements, metasurfaces can break the fundamental limitations of passive and static systems [39].

For reflecting and transmitting surfaces, reconfigurability implies the possibility of re-routing an incident beam, functionality which is seen as a key enabler for the envisioned next generation of communication networks (6G): walls, building, ceilings, and objects' external surfaces lose their status of electromagnetic obstacles for the wireless signals and become smart electromagnetic relay nodes [84].

Later on, these reprogrammable metasurface could also evolve to be software defined and even cognitive [37]. This concept, however, does not appear mature yet, despite the considerable amount of technical literature devoted to this topic, with only a few limited-scale prototypes realized so far. As a matter of fact, the introduction of tunability can limit performances (increase loss, limit bandwidth, etc) and result in complex control (tuning, biasing, etc) circuitry. Mechanisms such as externally controllable circuit components (varactors, pin diodes) [85]–[89] and tunable materials [90]–[92] have been investigated for dynamic reconfigurability. Circuit based approaches face scaling challenges in electrically large MTSs. With increased size, the number of components dramatically increases, along with cost and losses, if deep subwavelength cell dimensions are maintained. Liquid crystal layers are scalable, and have shown promising results at millimeter waves. However, they are relatively slow with millisecond response times. On the other hand, phase changing materials suffer from temperature instability. Alternative strategies make use of optical pumping of silicon or gallium arsenide substrates to alter the electrical properties of the inclusions [95].

Losses become less critical when dealing with a mechanical reconfiguration [93], [94]. Micromechanical systems or piezoelectric devices, however, may suffer from low reliability and be too sensitive to the external vibrations. As for the complexity of the control circuitry, questions remain on how such circuitry can be incorporated without interfering with the microwave/millimeter wave performance of the metasurface.

Space-time-modulated metastructures may also produce many novel physical phenomena and interesting applications, including optical isolators, breaking the Lorentz reciprocity, Doppler cloaks, harmonic generations, nonreciprocal antennas, full-duplex systems, and frequency conversion [96]. Most of these effects, however, are up to now only based on theoretical and/or numerical investigations, and experimental realizations remain limited.

VI. CONCLUSION

Modulated MTSs realized in PCB technology have emerged in the last years as a promising platform for low-loss planar devices in the microwave range. In fact, they are able to mold electromagnetic fields by controlling the boundary conditions through a gradual variation of the constituent unit cells.

This paper has first discussed the homogenized impedance model, with particular attention to the analysis of bound waves supported by this kind of MTSs. Then, different applications involving SW manipulation and SW-to-LW conversion have been reviewed, illustrating the design procedure and some practical realizations. The discussion was mainly focused on passive MTSs, however, additional degrees of freedom can be obtained by adding reconfigurability to these MTSs. This is an emerging topic with extremely stimulating perspectives.

ACKNOWLEDGMENT

The authors would like to thank the company Wave Up for providing the antenna patterns reported in Section IV C.

REFERENCES

[1] C. L. Holloway, E. F. Kuester, J. A. Gordon, J. O'Hara, J. Booth, and D. R. Smith, "An overview of the theory and applications of metasurfaces: The two-dimensional equivalents of metamaterials," *IEEE Antennas Propag. Mag.*, vol. 54, no. 2, pp. 10–35, Apr. 2012.

[2] F. Capolino, *Metamaterials Handbook 2: Applications of Metamaterials*. Boca Raton, CA, USA: CRC Press, 2009.

[3] C. L. Holloway, E. F. Kuester, and A. Dienstfrey, "Characterizing metasurfaces/metafilms: The connection between surface susceptibilities and effective material properties," *IEEE Antennas Wireless Propag. Lett.*, vol. 10, pp. 1507–1511, 2011.

[4] K. Achouri, M. A. Salem, and C. Caloz, "General metasurface synthesis based on susceptibility tensors," *IEEE Trans. Antennas Propag.*, vol. 63, no. 7, pp. 2977–2991, Jul. 2015.

[5] C. L. Holloway, D. C. Love, E. F. Kuester, J. A. Gordon, and D. A. Hill, "Use of generalized sheet transition conditions to model guided waves on metasurfaces/metafilms," *IEEE Trans. Antennas Propag.*, vol. 60, no. 11, pp. 5173–5186, Nov. 2012.

[6] B. H. Fong, J. S. Colburn, J. J. Ottusch, J. L. Visher, and D. F. Sievenpiper, "Scalar and tensor holographic artificial impedance surfaces," *IEEE Trans. Antennas Propag.*, vol. 58, no. 10, pp. 3212–3221, Oct. 2010.

[7] D. González-Ovejero, N. Chahat, R. Sauleau, G. Chattopadhyay, S. Maci, and M. Ettorre, "Additive manufactured metal-only modulated metasurface antennas," *IEEE Trans. Antennas Propag.*, vol. 66, no. 11, pp. 6106–6114, Nov. 2018.

[8] M. Patel and A. Grbic, "Modeling and analysis of printed-circuit tensor impedance surfaces," *IEEE Trans. Antennas Propag.,* vol. 61, no. 1, pp. 211–220, Jan. 2013.

[9] Y. Ye and S. He, "90° polarization rotator using a bilayered chiral metamaterial with giant optical activity," *Appl. Phys. Lett.*, vol. 96, no. 20, 2010, Art. no. 203501.

[10] C. Pfeiffer and A. Grbic, "Bianisotropic metasurfaces for optimal polarization control: Analysis and synthesis," *Phys. Rev. Appl.*, vol. 2, no. 4, Oct. 2014, Art. no. 044011.

[11] S. Sajuyigbe, M. Ross, P. Geren, S. A. Cummer, M. H. Tanielian, and D. R. Smith, "Wide angle impedance matching metamaterials for waveguide-fed phased-array antennas," *IET Microw. Antennas Propag.*, vol. 4, no.no. 8, pp. 1063–1072, 2010.

[12] T. R. Cameron and G. V. Eleftheriades, "Analysis and characterization of a wide-angle impedance matching metasurface for dipole phased arrays," *IEEE Trans. Antennas Propag.*, vol. 63, no. 9, pp. 3928–3938, Sep. 2015.

[13] M. Ebrahimpouri, L. F. Herran, and O. Quevedo-Teruel, "Wide-angle impedance matching using glide-symmetric metasurfaces," *IEEE Microw. Wireless Compon. Lett.*, vol. 30, no. 1, pp. 8–11, Jan. 2020.

[14] Y. Cheng, H. Yang, Z. Cheng, and B. Xiao, "A planar polarization-insensitive metamaterial absorber," *Photon. Nanostruct., Fundam. Appl.,* vol. 9, no. 1, pp. 8–14, Feb. 2011.

[15] D. Sievenpiper, Lijun Zhang, R. F. J. Broas, N. G. Alexopolous, and E. Yablonovitch, "High-impedance electromagnetic surfaces with a forbidden frequency band," *IEEE Trans. Microw. Theory Techn.*, vol. 47, no. 11, pp. 2059–2074, Nov. 1999.

[16] P. S. Kildal, E. Lier, and J. A. Aas, "Artificially soft and hard surfaces in electromagnetics and their application," in *Antennas Propag. Soc. Int. Symp. Dig.*, 1988, pp. 832–835.

[17] C. Pfeiffer and A. Grbic, "Millimeter-wave transmitarrays for wavefront and polarization control," *IEEE Trans. Microw. Theory Techn.*, vol. 61, no. 12, pp. 4407–4417, Dec. 2013.

[18] V. S. Asadchy, M. Albooyeh, S. N. Tcvetkova, A. Díaz-Rubio, Y. Ra'di, and S. A. Tretyakov, "Perfect control of reflection and refraction using spatially dispersive metasurfaces," *Phys. Rev. B*, vol. 94, no. 4, Aug. 2016, Art. no. 075142.

[19] E. M. Benini *et al.*, "Phase-gradient meta-dome for increasing grating-lobe-free scan range in phased arrays," *IEEE Trans. Antennas Propag.*, vol. 66, no. 8, pp. 3973–3982, Aug. 2018.

[20] V. G. Ataloglou, M. Chen, M. Kim, and G. V. Eleftheriades, "Microwave Huygens' metasurfaces: Fundamentals and applications," *IEEE J. Microwaves*, vol. 1, no. 1, pp. 374–388, Jan. 2021.

[21] Y. Yang *et al.*, "Full-polarization 3D metasurface cloak with preserved amplitude and phase," *Adv. Mater.*, vol. 28, no. 32, pp. 6866–6871, 2016.

[22] A. Alù, "Mantle cloak: Invisibility induced by a surface," *Phys. Rev. B*, vol. 80, no. 24, Dec. 2009, Art. no. 245115.

[23] J. Hunt *et al.*, "Metamaterial apertures for computational imaging," *Science,* vol. 18, no. 6117, pp. 310–313, Jan. 2013.

[24] M. F. Imani *et al.*, "Review of metasurface antennas for computational microwave imaging," *IEEE Trans. Antennas Propag.*, vol. 68, no. 3, pp. 1860–1875, Mar. 2020.

[25] D. J. Gregoire and A. V. Kabakian, "Surface-wave waveguides," *IEEE Antennas Wireless Propag. Lett.*, vol. 10, pp. 1512–1515, 2011.

[26] R. Quarfoth and D. Sievenpiper, "Artificial tensor impedance surface waveguides," *IEEE Trans. Antennas Propag.*, vol. 61, no. 7, pp. 3597–3606, Jul. 2013.

[27] R. C. Mitchell-Thomas, T. M. McManus, O. Quevedo-Teruel, S. A. R. Horsley, and Y. Hao, "Perfect surface wave cloaks," *Phys. Rev. Lett.*, vol. 111, no. 21, p. 213901, Nov. 2013.

[28] R. Quarfoth and D. Sievenpiper, "Surface wave scattering reduction using beam shifters," *IEEE Antennas Wireless Propag. Lett.*, vol. 13, pp. 963–966, 2014.

[29] C. Pfeiffer and A. Grbic, "A printed, broadband luneburg lens antenna," *IEEE Trans. Antennas Propag.*, vol. 58, no. 9, pp. 3055–3059, Sept. 2010.

[30] M. Bosiljevac, M. Casaletti, F. Caminita, Z. Sipus, and S. Maci, "Non-uniform metasurface Luneburg lens antenna design," *IEEE Trans. Antennas Propag.*, vol. 60, no. 9, pp. 4065–4073, Sep. 2012.

[31] M. Huang, S. Yang, F. Gao, R. Quarfoth, and D. Sievenpiper, "A 2-D multibeam half Maxwell fish-eye lens antenna using high impedance surfaces," *IEEE Antennas Wireless Propag. Lett.*, vol. 13, pp. 365–368, 2014.

[32] O. Quevedo-Teruel, J. Miao, M. Mattsson, A. Algaba-Brazalez, M. Johansson, and L. Manholm, "Glide-symmetric fully metallic luneburg lens for 5G communications at Ka-band," *IEEE Antennas Wireless Propag. Lett.*, vol. 17, no. 9, pp. 1588–1592, Sep. 2018.

[33] J. Ruiz-García, E. Martini, C. D. Giovampaola, D. González-Ovejero, and S. Maci, "Reflecting Luneburg lenses," *IEEE Trans. Antennas Propag.*, vol. 69, no. 7, pp. 3924–3935, Jul. 2021.

[34] A. M. Patel and A. Grbic, "A printed leaky-wave antenna based on a sinusoidally-modulated reactance surface," *IEEE Trans. Antennas Propag.*, vol. 59, no. 6, pp. 2087–2096, Jun. 2011.

[35] G. Minatti *et al.*, "Modulated metasurface antennas for space: Synthesis, analysis and realizations," *IEEE Trans. Antennas Propag.*, vol. 63, no. 4, pp. 1288–1300, Apr. 2015.

[36] M. Faenzi *et al.*, "Metasurface antennas: New models, applications and realizations," *Sci. Reps*, vol. 9, no. 1, Jul. 2019, Art. no. 10178.

[37] L. Zhang *et al.*, "Space-time-coding digital metasurfaces," *Nature Commun.,* vol. 9, 2018, Art. no. 4334.

[38] F. Liu *et al.*, "Intelligent metasurfaces with continuously tunable local surface impedance for multiple reconfigurable functions," *Phys. Rev. Appl.*, vol. 11, no. 4, Apr. 2019, Art. no. 044024.

[39] A. Li, Z. Luo, H. Wakatsuchi, S. Kim, and D. F. Sievenpiper, "Nonlinear, active, and tunable metasurfaces for advanced electromagnetics applications," *IEEE Access*, vol. 5, pp. 27439–27452, 2017.

[40] M. Chen, M. Kim, A. M. H. Wong, and G. V. Eleftheriades, "Huygens' metasurfaces from microwaves to optics: A review," *Nanophotonics*, vol. 7, no. 6, 2018, pp. 1207–1231.

[41] F. Yang *et al.*, "Antireflection and wavefront manipulation with cascaded metasurfaces," *Phys. Rev. Appl.*, vol. 14, no. 6, Dec. 2020, Art. no. 064044.

[42] F. Liu *et al.*, "Intelligent metasurfaces with continuously tunable local surface impedance for multiple reconfigurable functions," *Phys. Rev. Appl.*, vol. 11, Apr. 2019, Art. no. 044024.

[43] C. Elachi, "Waves in active and passive periodic structures: A review," *Proc. IEEE*, vol. 64, no. 12, pp. 1666–1698, Dec. 1976.

[44] M. A. Francavilla, E. Martini, S. Maci, and G. Vecchi, "On the numerical simulation of metasurfaces with impedance boundary condition integral equations," *IEEE Trans. Antennas Propag.*, vol. 63, no. 5, pp. 2153–2161, May 2015.

[45] E. Martini, F. Caminita, and S. Maci, "Double-scale homogenized impedance models for periodically modulated metasurfaces," *EPJ Appl. Metamater.*, vol. 7, no. 12, 2020, Art. no. 8.

[46] S. Maci and A. Cucini, "FSS-based EBG surface," in *Electromagnetic Metamaterials: Physics and Engineering Aspects*, N. Engheta and R. Ziolkowski, Eds. Hoboken, NJ, USA: Wiley, 2006.

[47] C. Yepes, M. Faenzi, S. Maci, and E. Martini, "Perfect non-specular reflection with polarization control by using a locally passive metasurface sheet on a grounded dielectric slab," *Appl. Phys. Lett.*, vol. 118, no. 23, 2021, Art. no. 231601.

[48] J. P. S. Wong, A. Epstein, and G. V. Eleftheriades, "Reflectionless wide-angle refracting metasurfaces," *IEEE Antennas Wireless Propag. Lett.*, vol. 15, pp. 1293–1296, 2016, doi: 10.1109/LAWP.2015.2505629.

[49] A. M. Patel and A. Grbic, "The effects of spatial dispersion on power flow along a printed-circuit tensor impedance surface," *IEEE Trans. Antennas Propag.*, vol. 62, no. 3, pp. 1464–1469, Mar. 2014.

[50] M. Mencagli, E. Martini, and S. Maci, "Surface wave dispersion for anisotropic metasurfaces constituted by elliptical patches," *IEEE Trans. Antennas Propag.*, vol. 63, no. 7, Jul. 2015, pp. 2992–3003.

[51] O. Lukkonen *et al.*, "Simple and accurate analytical model of planar grids and high-impedance surfaces comprising metal strips or patches," *IEEE Trans. Antennas Propag.*, vol. 56, no. pp. 6 pp. 1624–1632, Jun. 2008.

[52] D. Ramaccia, A. Toscano, and F. Bilotti, "A new accurate model of high impedance surfaces consisting of circular patches," *Prog. Electromagn. Res. M*, vol. 21, pp. 1–17, 2001.

[53] M. Lucido, F. Schettino, M. D. Migliore, D. Pinchera, F. Di Murro, and G. Panariello, "Electromagnetic scattering by a zero-thickness PEC annular ring: A new highly efficient MoM solution," *J. Electromagn. Waves Appl.*, vol. 31, no. 4, 2017, pp. 405–416.

[54] D. González-Ovejero and S. Maci "Gaussian ring basis functions for the analysis of modulated metasurface antennas," *IEEE Trans. Antennas Propag.*, vol. 63, no. 9, pp. 3982–3993, Sep. 2015.

[55] M. Bodehou, D. González-Ovejero, C. Craeye, and I. Huynen, "Method of moments simulation of modulated metasurface antennas with a set of orthogonal entire-domain basis functions," *IEEE Trans. Antennas Propag.*, vol. 67, no. 2, pp. 1119–1130, Feb. 2019.

[56] D. González-Ovejero, G. Chattopadhyay, and S. Maci, "Efficient analysis of metasurfaces in a planar layered medium," in *Proc. IEEE Int. Symp. Antennas Propag. USNC/URSI Nat. Radio Sci. Meeting*, 2015, pp. 1082–1083.

[57] F. Vernì, M. Righero, and G. Vecchi, "On the use of entire-domain basis functions and fast factorizations for the design of modulated metasurface," *IEEE Trans. Antennas Propag.*, vol. 68, no. 5, pp. 3824–3833, May 2020.

[58] F. Caminita, E. Martini, G. Minatti, and S. Maci, "Fast integral equation method for metasurface antennas," *Proc. URSI Int. Symp. Electromagn. Theory*, 2016, pp. 480–483.

[59] D. J. Bisharat and D. F. Sievenpiper, "Electromagnetic-dual metasurfaces for topological states along a 1D interface," *Laser Photon. Rev.*, vol. 13, no. 10, 2019, Art. no. 1900126.

[60] E. Martini, M. G. Silveirinha, and S. Maci, "Exact solution for the protected TEM edge mode in a PTD-symmetric parallel-plate waveguide," *IEEE Trans. Antennas Propag.*, vol. 67, no. 2, pp. 1035–1044, Feb. 2019.

[61] E. Martini, M. Mencagli, D. Gonzalez-Ovejero, and S. Maci, "Flat optics for surface waves," *IEEE Trans. Antennas Propag.*, vol. 64, no. 1, pp. 155–166, Jan. 2016.

[62] D. R. Prado, A. V. Osipov, and O. Quevedo-Teruel, "Implementation of transformed lenses in bed of nails reducing refractive index maximum value and sub-unity regions," *Opt. Lett.*, vol. 40, pp. 926–929, 2015.

[63] M. Mencagli, E. Martini, D. González-Ovejero, and S. Maci, "Metasurfing by transformation electromagnetics," *IEEE Antennas Wireless Propag. Lett.*, vol. 13, pp. 1767–1770, 2014.

[64] E. Martini, M. Mencagli, and S. Maci, "Metasurface transformation for surface wave control," *Philos. Trans. Roy. Soc. A*, vol. 373, no. 2049, Jul. 2015, Art. no. 20140355.

[65] A. M. Patel and A. Grbic, "Transformation electromagnetics devices based on printed-circuit tensor impedance surfaces," *IEEE Trans. Microw. Theory Techn.*, vol. 62, no. 5, pp. 1102–1111, May 2014.

[66] E. Martini and S. Maci, "Metasurface transformation theory," in *Transformation Electromagnetics and Metamaterials*, D. H. Werner and D. H. Know, Eds. New York, NY, USA: Springer, 2013, pp. 83–116.

[67] M. Mencagli, E. Martini, D. González-Ovejero, and S. Maci "Metasurface transformation optics," *J. Opt.*, vol. 16, no. 12, 2014, Art. no. 125106.

[68] B. Pendry, D. Schurig, and D. R. Smith, "Controlling electromagnetic fields," *Science*, vol. 312, pp. 1780–1782, Jun. 2006

[69] D. Kwon and D. H. Werner, "Transformation electromagnetics: An overview of the theory and applications," *IEEE Antennas Propag. Mag.*, vol. 52, no. 1, pp. 24–46, Feb. 2010.

[70] R. Quarfoth and D. Sievenpiper, "Surface wave scattering reduction using beam shifters," *IEEE Antennas Wireless Propag. Lett.*, vol. 13, pp. 963–966, 2014.

[71] X. Wan, X. Shen, Y. Luo, and T. J. Cui, "Planar bifunctional Luneburg-fisheye lens made of an anisotropic metasurface," *Laser Photon. Rev.*, vol. 8, no. 5, pp. 757–765, 2014.

[72] M. Caiazzo, S. Maci, and N. Engheta, "A metamaterial surface for compact cavity resonators," *IEEE Antennas Wireless Propag. Lett.*, vol. 3, pp. 261–264, 2004.

[73] S. N. Tcvetkova, S. Maci, and S. A. Tretyakov, "Exact solution for conversion of surface waves to space waves by periodical impenetrable metasurfaces," *IEEE Trans. Antennas Propag.*, vol. 67, no. 5, pp. 3200–3207, May 2019.

[74] S. N. Tcvetkova, E. Martini, S. A. Tretyakov, and S. Maci, "Perfect conversion of a TM surface wave into a TM leaky wave by an isotropic periodic metasurface printed on a grounded dielectric slab," *IEEE Trans. Antennas Propag.*, vol. 68, no. 8, pp. 6145–6153, Aug. 2020.

[75] N. Raveu, B. Byrne, L. Claudepierre, and N. Capet, "Modal theory for waveguides with anisotropic surface impedance boundaries," *IEEE Trans. Microw. Theory Techn.*, vol. 64, no. 4, pp. 1153–1162, Apr. 2016.

[76] Q. Wu *et al.*, "A Ku-band dual polarization hybrid-mode horn antenna enabled by printed-circuit-board metasurfaces," *IEEE Trans. Antennas Propag.*, vol. 61, no. 3, pp. 1089–1098, Mar. 2013.

[77] M. Faenzi, D. González-Ovejero, and S. Maci, "Wideband active region metasurface antennas," *IEEE Trans. Antennas Propag.*, vol. 68, no. 3, pp. 1261–1272, Mar. 202.

[78] V. Sozio *et al.*, "Design and realization of a low cross-polarization conical horn with thin metasurface walls," *IEEE Trans. Antennas Propag.*, vol. 68, no. 5, pp. 3477–3486, May 2020.

[79] A. Oliner and A. Hessel, "Guided waves on sinusoidally-modulated reactance surfaces," *IRE Trans. Antennas Propag.*, vol. 7, no. 5, pp. 201–208, Dec. 1959.

[80] F. Caminita, E. Martini, and S. Maci, "Exact solution for anysotropic, periodically modulated boundary conditions excited by a surface wave," in *Proc. 9th Eur. Conf. Antennas Propag.*, 2015, Art. no. 51687900.

[81] G. Minatti, F. Caminita, E. Martini, and S. Maci, "Flat optics for leaky waves on modulated metasurfaces: Adiabatic floquet-wave analysis," *IEEE Trans. Antennas Propag.*, vol. 64, no. 9, pp. 3896–3906, Sep. 2016.

[82] G. Minatti, F. Caminita, E. Martini, M. Sabbadini, and S. Maci, "Synthesis of modulated-metasurface antennas with amplitude, phase, and polarization control," *IEEE Trans. Antennas Propag.*, vol. 64, no. 9, pp. 3907–3919, Sep. 2016.

[83] M. Bodehou, C. Craeye, E. Martini, and I. Huynen, "A quasi-direct method for the surface impedance design of modulated metasurface antennas," *IEEE Trans. Antennas Propag.*, vol. 67, no. 1, pp. 24–36, Jan. 2019.

[84] M. Di Renzo *et al.*, "Smart radio environments empowered by reconfigurable intelligent surfaces: How it works, state of research, and the road ahead," *IEEE J. Sel. Areas Commun.*, vol. 38, no. 11, pp. 2450–2525, Nov. 2020.

[85] K. Chen *et al.*, "A reconfigurable active Huygens' metalens," *Adv. Mater.*, vol. 29, no. 17, 2017, Art. no. 1606422.

[86] M. Kim and G. V. Eleftheriades, "Guided-wave-excited binary huygens' metasurfaces for dynamic radiated-beam shaping with independent gain and scan-angle control," *Phys. Rev. Appl.*, vol. 15, no. 5, May 2021, Art. no. 054037.

[87] Y. Li, Y. Wang, and Q. Cao, "Design of a multifunctional reconfigurable metasurface for polarization and propagation manipulation," *IEEE Access*, vol. 7, pp. 129183–129191, 2019.

[88] C. Mias and J. H. Yap, "A varactor-tunable high impedance surface with a resistive-lumped-element biasing grid," *IEEE Trans. Antennas Propag.*, vol. 55, no. 7, pp. 1955–1962, Jul. 2007.

[89] B. Ratni, A. de Lustrac, G.-P. Piau, and S. N. Burokur, "Reconfigurable meta-mirror for wavefronts control: Applications to microwave antennas," *Opt. Exp.*, vol. 26, no. 3, pp. 2613–2624, 2018.

[90] S. Foo, "Liquid-crystal reconfigurable metasurface reflectors," in *Proc. IEEE Int. Symp. Antennas Propag. USNC/URSI Nat. Radio Sci. Meeting*, 2017, pp. 2069–2070.

[91] J. Shabanpour, S. Beyraghi, and A. Cheldavi, "A ultrafast reprogrammable multifunctional vanadium-dioxide-assisted metasurface for dynamic THz wavefront engineering," *Sci Rep.*, vol. 10, no. 1, 2020, Art. no. 8950.

[92] H. Chen, W.-B. Lu, Z.-G. Liu, and M.-Y. Geng, "Microwave programmable graphene metasurface," *ACS Photon.*, vol. 7, no. 6, pp. 1425–1435, 2020.

[93] H. Rajagopalan, Y. Rahmat-Samii, and W. A. Imbriale, "RF MEMS actuated reconfigurable reflectarray patch-slot element," *IEEE Trans. Antennas Propag.*, vol. 56, no. 12, pp. 3689–3699, Dec. 2008.

[94] M. Mavridou, A. P. Feresidis, G. P. Hall, and S. Peter, "Tunable millimetre-wave phase shifting surfaces using piezoelectric actuators," *IET Microw., Antennas Propag.*, vol. 8, no. 11, pp. 829–834, 2014.

[95] E. M. González-Ovejero, B. Loiseaux, C. Tripon-Canseliet, M. Mencagli, jr., J. Chazelas, and S. Maci, "Basic properties of checkerboard metasurfaces," *IEEE Antennas Wireless Propag. Lett.*, vol. 14, pp. 406–409, 2015.

[96] D. Ramaccia, D. L. Sounas, A. Alù, A. Toscano, and F. Bilotti, "Phase-induced frequency conversion and Doppler effect with time-modulated metasurfaces," *IEEE Trans. Antennas Propag.*, vol. 68, no. 3, pp. 1607–1617, Mar. 2020.